Interdecadal Variability of Southeastern South America Rainfall and Moisture Sources during the Austral Summertime

VERÓNICA MARTÍN-GÓMEZ

Instituto de Física. Universidad de la República, Montevideo (Uruguay)

EMILIO HERNÁNDEZ-GARCIA

IFISC (CSIC-UIB) - Instituto de Física interdisciplinar y Sistemas Complejos, Campus Universitat de les Illes Balears. E-07122. Palma de Mallorca (Spain)

MARCELO BARREIRO

Instituto de Física. Universidad de la República, Montevideo (Uruguay)

CRISTÓBAL LÓPEZ

IFISC (CSIC-UIB) - Instituto de Física interdisciplinar y Sistemas Complejos, Campus Universitat de les Illes Balears. E-07122. Palma de Mallorca (Spain)

1. Introduction

This study focuses on Southeastern South America (SESA), a region that covers Uruguay and portions of northeastern Argentina and South Brazil (see Table 1 and Figure 1). SESA corresponds mostly to the southern part (south of 25S) of the La Plata Basin (LPB), the second largest basin in South America which comprehends parts of Brazil, Paraguay, Uruguay, Argentina and Bolivia. SESA, located to the south of the Amazon basin, is one of the most densely populated regions in South America. Precipitation and its variability is very important over the region because it plays a key role in the generation of hydroelectric energy and in the economy, which is mainly based on harvesting and ranching (Berbery and Barros 2002). Moisture that could lead to future precipitations over the region can come from two different sources: (i) water vapor advection from others regions, and/or (ii) local recycling. While the advection of

water vapor depends on the atmospheric circulation and can have two different origins (continental or oceanic), the recycling is the process by which evapotranspiration from a particular continental region returns as precipitation to it shelf (Brubaker et al. 1993).

Previous moisture studies have focused mainly on the whole LPB and are described below for reference. One of the goals of this study is then to assess how much of the previous results found for the whole LPB apply to SESA. According to Martinez and Dominguez, 2014, approximately 63% of the mean precipitation over LPB comes from South America and the remaining 37% comes mostly from southern Pacific and Atlantic Oceans. Studies have also shown that the main continental moisture source of LPB is the Amazon Basin (e.g., Martinez and Dominguez 2014; Zemp et al. 2014; Drumond et al. 2014; Dirmeyer et al. 2009; Barros and Berbery 2002), contributing with 24% of the annual mean precipitation over LPB (Martinez and Dominguez, 2014). Using the concept of cascading moisture recycling, which represents the moisture transport between two locations on the continent that evolves one or more re-evaporation cycles along the way, Zemp et al. 2014 showed that the southern Amazon could act not only as the main direct continental moisture source of LPB, but also as an intermediate region that distributes moisture originating from the entire Amazon basin during the wet season (December to March). The transport of the southern Amazonian moisture toward LPB takes place throughout the year, being a quasi-permanent source with a maximum during the austral summer season (Berbery and Barros, 2002; Martinez and Dominguez 2014). The transport is carried out via the South American Low Level Jet (SALLJ) along the Andes (Marengo 2005; Martinez and Dominguez, 2014).

Another continental type of moisture source but without advection from other regions is the local recycling. For LPB, it represents the 23.5% of its total annual mean precipitation and becomes its maximum during the austral summer season due to the

enhancement of the large-scale convergence and net radiation, which increases the atmospheric instability, precipitation and evaporation (Martinez and Dominguez 2014).

The Atlantic and Pacific oceans are the main oceanic moisture sources of LPB and are seasonally dependent (Drumond et al. 2008; Martinez and Dominguez 2014). Drumond et al. 2008 used a Lagrangian particle dispersion model to compute the trajectories of the particles in the atmosphere backwards in time. They focused mainly on SESA and found that its main oceanic moisture sources are the southwestern South Atlantic, the tropical north Atlantic and the surrounding Atlantic Ocean located eastern to central Brazil. While the two latter remain as moisture sources throughout the year, the moisture from the tropical north Atlantic only reaches LPB during the austral summer season. This is associated with the development of a cross equatorial flow carrying moisture from the north Atlantic that penetrates into South America. Over the continent, the presence of the Andes forces the flow to become northerly, and is channeled southwards reaching LPB (Drumond et al. 2008; Martinez and Dominguez 2014; Viviane et al. 2012).

Regarding the Pacific Ocean, Martinez and Dominguez, 2014 showed that the subtropical and extratropical part of the south Pacific contributes to LPB precipitation with a 7.1% of the total annual mean precipitation, being its contribution more important during the austral winter.

It is well known that the atmospheric circulation is sensitive to the ocean surface conditions in the tropics. Anomalies in the sea surface temperature (SST) over the tropical oceans are able to induce changes in the meridional circulation and generate stationary Rossby waves that propagate toward extratropical latitudes, processes that induce variations in the regional circulation patterns associated to rainfall.

For the particular case of SESA, several previous studies have shown that the SST anomalies in the tropical Pacific, Atlantic and Indian oceans can influence precipitation variability through atmospheric teleconnections (e.g., Seager et al. 2010; Barreiro et al. 2014; Grimm et al. 2000; Silvestri 2004; Barreiro 2010; Diaz et al. 1998 and Chan et al. 2008) and they also the moisture transport (e.g., Silva et al. 2009; Vera 2004; Martinez and Dominguez 2014; Castillo 2014).

El Niño-Southern Oscillation (ENSO) is one of the interannual variability phenomena that has been shown to influence the moisture transport from the Amazon Basin toward LPB through changes in the intensity of the SALLJ (Silva et al. 2009; Vera 2004; Martinez and Dominguez 2014). The physical mechanism through which the positive phase of El Niño induces an increase of the moisture of Amazonian origin in LPB involves a weakening of the Walker circulation that increases anomalous subsidence over Brazil, which subsequently enhances upward motion over Southeastern South America (Andreoli and Kayano 2005). This weakening in the local Hadley circulation between tropical and subtropical South America turns into a strengthens of the southward transport of moisture in lower levels from Brazil toward SESA, which is related to a larger number of SALLJ intensification events during the positive phase of ENSO (Silva et al. 2009).

Moreover, the warm phase of this equatorial Pacific phenomenon has been shown to increase the moisture from the southern Pacific in LPB (Martinez and Dominguez 2014). Martinez and Dominguez, (2014) suggest that this could be due to the anomalous upper-level circulation pattern during the Niño events, where stronger subtropical westerlies occur together with an anomalous cyclone located over the southern Pacific along with an anomalous anticyclone over the southern Atlantic (Andreoli and Kayano 2005; Vera et al. 2004; Ropelewski and Halpert 1987).

Finally, the tropical oceans can interact with each other inducing SST anomalies in remote basins through atmospheric and oceanic teleconnections (e.g., Alexander et al. 2002; Enfield and Mayer 1997; Saravannan and Chang 2000; Rodriguez-Fonseca et al. 2009). Recently Martín-Gómez and Barreiro (2015) used a methodology borrowed from complex networks to study how SST anomalies in the three tropical oceans can work together to induce springtime rainfall variability over SESA. Here we extend that study focusing on the summer season and find that there is a strong decadal variability in the impact of the oceans on SESA rainfall accompanied by large changes in moisture sources.

This study comprehends two parts: one first part in which following the methodology of Tsonis et al. (2007) and Martín-Gómez and Barreiro (2015), we construct a climate network in order to detect different synchronization periods among the tropical oceans and the precipitation over SESA, understanding synchronization as those periods over the last century in which several (or in the best case all) of the network's nodes are significantly interacting among them. In the second part we select two periods with different degree of synchronization and, employing a Lagrangian particle dispersion model, we calculate and compare the trajectories of atmospheric moisture in both cases. This provides information about the spatial distribution of the moisture sources of SESA in the two selected periods and allows analyzing their changes.

2. Construction of the climate network and synchronization measure

A climate network is constructed considering as network's nodes the following five different tropical oceanic indices (see Fig. 1 an Table 1): El Niño3.4, Tropical North Atlantic (TNA), Tropical South Atlantic (TSA), Equatorial Atlantic (ATL3) and Indian Ocean Dipole (IOD), as well as a precipitation index over SESA (PCP SESA). The

election of the indices takes into account all the tropical basins that are known to influence SESA precipitation during the austral summertime. The oceanic indices are defined considering the monthly mean SST from the Extended Reconstructed Sea Surface Temperature database (ERSSTv3b; Smith et al. 2008; and Xue et al. 2003) with a resolution of 2º x 2º. The precipitation index is defined using the monthly mean observed data from the GPCCv5 (Global Precipitation Climatology Center; Schneider et al. 2011) with a resolution of 1º x 1º. The period of study is 1901-2005.

We also consider the monthly mean values of the vertical integral of the horizontal divergence of the moisture flux from ECMWF ERA-Interim reanalysis data, of the winds at 850hPa and of the geopotential at 200hPa obtained from ECMWF data server (Dee et al. 2011). These fields are used to diagnose circulation anomalies and understand the changes in the moisture sources for SESA in different periods. The available data span the period 1979-to present, so to compute the anomaly values of all the products from ERA-Interim employed in this work (vertical integral of the horizontal divergence of the moisture flux, winds at 850hPa and geopotential at 200hPa), we consider the climatological mean from the common period (1979-2005).

The methodology followed to construct the network is described in detail in Martín-Gómez and Barreiro, 2015. Here we provide a summarized version. It consists in several steps:

1) The climate indices are defined by spatially averaging the SST or precipitation anomalies in the respective regions (Table 1) within individual trimesters: September – November (SON) for the case of El Niño3.4 index and December – February (DJF) for the other indices (TNA, TSA, ATL3, IOD and PCP). In this situation, each one of the time series values represents the seasonal mean of the

monthly anomaly values of the SST (tropical oceanic regions) or PCP (SESA region, only land areas). The anomaly values of the indices were computed as the deviation from the monthly climatological mean during the period (1901-2005). Therefore, our time series have 105 values, one per year. Each time series will be a node in a climate network.

The lag time of 3 months among El Niño3.4 and the rest of the nodes was established in order to allow them to respond to the atmospheric anomalies generated by the equatorial Pacific.

2) For each year, a climate network is constructed by computing the Spearman correlation coefficient ρ_{ij}^{t} among each pair i,j of time series in the interval [$t-\frac{\Delta t}{2}$, $t+\frac{\Delta t}{2}$]. This correlation is a measure of the strength of the connection between the corresponding pair of nodes at the time t in the middle of a sliding window of length Δt=11 years. The mean network distance is computed as a measure of synchronization among the nodes:

$$d(t)=\frac{2}{N(N-1)}\sum_{i<j}\sqrt{2\left(1-\left|\rho_{ij}^{t}\right|\right)}, \quad (1)$$

where N is the number of network's nodes (in this case, 6) Note that the network is completely synchronized when the distance is zero and uncorrelated nodes give a value of $\sqrt{2}$ to the distance.

3) To compute the statistical significance of the mean network distance we employ the Montecarlo Method under the following criterion: we consider a red noise null model for those nodes with autocorrelation coefficient at lag 1 significant at 95% level in a one-tailed t-test. In the opposite case we consider white noise.

Following this criterion, only the TNA and TSA can be considered as red noise. Then, we generate 1000 surrogate time series of each index under these null hypotheses and compute the network distance time series considering a sliding window of 11-years length. In this way, we construct 1000 surrogate time series of the mean network distance, which allows determining the 5% significance level. We consider that there is a statistically significant synchronization event when the mean network distance is below this threshold more than 7 consecutive years.

3. Lagrangian Model and identification of moisture sources.

To get information about the spatial distribution of the moisture sources of SESA, we consider a Lagrangian particle dispersion model (FLEXPART, Stohl et al. 2005) driven by the 6 hours forecast from Climate Forecast System Reanalysis (NCEP-CFSR, Saha et al. 2010) with a resolution of 0.5º x 0.5º during the period 1979 to 2000. We consider the NCEP-CFSR data because this reanalysis is able to reproduce correctly the lower and upper-level atmospheric circulation patterns and precipitation distribution over South America during the austral summer season (Viviane et al. 2012; Quadro et al. 2013).

FLEXPART is a Lagrangian Particle dispersion model able to calculate and track the trajectories of the atmospheric moisture running forward and backward in time while dividing the atmosphere into a large number of particles (Stohl et al. 2005). Each particle represents a mass of air with a given mass (m) which is transported by the 3D wind field which includes modelled turbulence. In our work, the vertical distribution of the particles in the atmosphere is proportional to the air density and the moisture sources are computed through the net budget of evaporation minus precipitation

obtained from the changes in the moisture along the particles trajectories. As in Stohl and James (2004, 2005) and in Drumond et al. (2008), the steps are:

1) We select the vertical atmospheric column located over SESA (see spatial domain on table 1), from where we release 50.000 particles per simulation with a vertical distribution proportional to the air density. We perform 5 simulations per month (December – January – February) releasing the particles the days: 12nd, 16th, 20th, 24th and 28th of each month. All these particles are transported by FLEXPART backwards in time for 10 days and tracked recording their positions and specific humidity every 6 hours. We limit the transport of the particles to 10 days because it represents the average time that the water vapor resides in the atmosphere (Numagutti 1999). In turn, we establish a lag time between consecutive simulations of 4 days in order to assure that the obtained particle trajectories are different in consecutives simulations, since the life-time of the synoptic perturbation is around 5 days.

2) The net budget evaporation (e) minus precipitation (p) of each particle *i* with mass '*m*' was computed through changes in the specific humidity (q) along its trajectory:

$$(e-p)_i = \left(m \cdot \frac{dq}{d\tau} \right)_i , \quad (2)$$

The $(e-p)_i$ parameter was calculated for specific days. We called $(e-p)_{i,n}$ to the net budget evaporation minus precipitation of the particle *i* during the *n*-th day of trajectory. Remember that we release the particles the 10th day of trajectory and run the model back in time, so for example $(e-p)_{i,1}$ will represent the net budget evaporation minus precipitation of the particle *i* during

the first day of trajectory, which is developed from day 10th to the day 9th. In general terms, this can be mathematically expressed as:

a. $$(e-p)_{i,n} = \left(m_i \frac{q_{i,day=(10-n+1)} - q_{i,day=(10-n)}}{\Delta\tau} \right) \quad (3)$$

where $\Delta\tau = 1$ day.

3) We define a (1º x 1º) grid and per each day of trajectory, we add $(e-p)_{i,n}$ for all the particles *'i'* of the vertical column located over an area A, obtaining the net budget $(E-P)_n$ for the whole vertical column of area A in each grid point and during the *n*-th day of trajectory:

$$(E-P)_n = \frac{\sum_{i;vertical\_column} (e-p)_{i,n}}{\sigma \cdot Area_{column}}, \quad (4)$$

where σ represents the density of the water. The expression (4) gives the net budget as equivalent height of water per unit of time.

4) Finally, we take the average of the 10 net budgets $(E-P)_n$, and call it $(E-P)^{10}$. Per each grid cell, the parameter $(E-P)^{10}$ will represent the net budget evaporation minus precipitation in the whole vertical column located over an area A (the area of the grid cell) averaged over the 10 days of trajectory of the particles going toward SESA (see equation (5)). The positive (negative) values of $(E-P)^{10}$ will represent the regions where particles when passing gain (loss) moisture in average over the 10 days of trajectory toward SESA, and therefore, these regions will represent sources (sinks) of moisture.

$$(E-P)^{10} = \frac{1}{10} \sum_{n=1}^{10} (E-P)_n, \quad (5)$$

4. Climate network and synchronization periods

Figure 2 shows the network distance (solid black line) and the PCP index on DJF (dashed black line) during the last century. Regarding the mean network distance, the major features are:

1) The network distance is characterized by interannual and interdecadal variability.

2) During the last century there were three synchronization periods (distance smaller than the significance level): (1934-1946), (1965-1975) and (1992-2000), marked by white bands in Figure 2.

The existence of synchronization periods indicates that several of the nodes in the network (or in the best case all) are interacting among them. However, this does not assure that during these periods the oceans are influencing rainfall over SESA. To address this question we compute the Spearman correlation coefficient between the mean network distance and a precipitation index over SESA constructed taking averages of 11 years sliding windows from SESA PCP index. The resulting correlation coefficient, -0.25, is statistically significant at 5% significance level in one sided t-test (threshold level is 0.17), suggesting that an increase of the network distance (a decrease in the synchronization among the network's nodes) is associated with less precipitation over SESA. The anti-correlation is evident in Figure 2. However, this result does not completely ensure the increment of SESA precipitation as a consequence of enhancing the degree of synchronization of the network. To further address this issue we define the relative precipitation weight (RPW), a parameter that informs about the importance of the PCP as a network's node, understanding "importance" as the degree of interaction of the precipitation index with the rest of the nodes. The definition of RPW(t) is:

$$RPW(t) = \frac{\frac{\sqrt{2}}{3} - d_{pcp}(t)}{\sqrt{2} - d(t)} \quad (6)$$

where d_{pcp} is proportional to the mean network distance from PCP to the tropical oceanic indices in equation (1). That is to say:

$$d_{pcp}(t) = \frac{2}{N(N-1)} \sum_{i \neq PCP} \sqrt{2\left(1 - \left|\rho^{t}_{i,PCP}\right|\right)} \quad (7)$$

where N=6 (the number of network's nodes) and $\rho^{t}_{i,PCP}$ is the Spearman correlation coefficient between PCP and the oceanic index i. The maximum and minimum values of the RPW are one and zero, in such a way that higher values of the RPW are associated with a larger influence of the tropical oceans on rainfall and vice versa. RPW=1 takes place when d_{pcp}=0 (correlation coefficient between each one of the oceanic indices and PCP index are 1 or -1) and the tropical oceans are completely disconnected among them. RPW=0 means that SESA precipitation is completely disconnected from the oceanic indices. See more details in Martín-Gómez and Barreiro, 2015.

The Spearman correlation coefficient between the RPW and the mean network distance, -0.22, is statistically significant at 5% significance level in a one sided t-test, suggesting that a larger connectivity of the precipitation index is associated with a smaller network distance (larger synchronization of the network). On the other hand, we also computed the correlation coefficient between the RPW and the precipitation, obtaining the value 0.24, also statistically significant at 5% significance level in a one sided t-test. These results suggest that an increment of the precipitation in SESA is related to a larger

influence of the tropical oceans on SESA, which in turn, is associated with more degree of synchronization.

So, one could conclude that more synchronization of the network is associated with an increase of the precipitation over SESA. Nevertheless, we note that there are periods in which precipitation is above normal but the network does not show significant synchronization, e.g. during the decades of 1910s and 1980s.

5. Moisture sources of SESA during the ‘80s and ‘90s.

Given the availability of ERA Interim and NCEP-CFSR data, we focus our discussion on the differences between the ‘80s (1979-1991) and ‘90s (1992-2000), a period of non-significant synchronization and another of statistically significant synchronization among network’s components, respectively. Note that reducing the period to 1979-2000, the ‘80s have rainfall below the mean, while the ‘90s have rainfall above the mean in SESA.

We first analyze SST and circulation anomalies in the two periods. The Spearman correlation map between the SESA precipitation index and the SST anomalies for the two periods, ‘80s and ‘90s, are shown in Figure 3. The shaded regions are statistically significant at 5% significance level in a MonteCarlo test based on the generation of 100 surrogate time series. The first distinctive feature between these two decades is that while in the ‘90s the equatorial Pacific dominates, during the ‘80s the equatorial Atlantic shows stronger correlation. The vertical integral of moisture flux divergence is consistent with increased rainfall over SESA during the 90s and decreased during the 80s (Figures 4(a) and (d)).

Figures 4 (b) and (e) show the anomalous eddy geopotential at 200mb during ‘80s and ‘90s, respectively. The ‘80s are characterized by an anomalous anticyclone located southeast of South America over the Atlantic Ocean and an anomalous cyclone over southern South America (Figure 4(b)). This situation does not favor the convergence of moisture over SESA and inhibits vertical ascent motions. However, during the ‘90s the subtropical dipole of cyclonic-anticyclonic circulation anomalies in subtropical South America favors the advection of cyclonic vorticity and ascent motion over SESA, and therefore, the increase of the precipitation. The low level wind anomalies are consistent with this picture, showing mainly divergence (convergence) over SESA during the 80s (90s) (see Figures 4(c) and (f)).

Figures 5 (a) and (b) represent the 10 days average of the net budget evaporation minus precipitation ($(E-P)^{10}$) over the periods (1979-1991) and (1992-2000), respectively. Regions with positive (negative) values of this variable are associated with a net profit (loss) of moisture of the particles when passing by along their trajectories toward SESA, and therefore, these regions will represent the main moisture sources (sinks) of SESA. From Figures 5 (a) and (b) we can see that the main moisture source regions (with positive values of the $(E-P)^{10}$) are: the recycling over SESA, the central-eastern shore of Brazil together with its surrounding Atlantic ocean, and the South Atlantic Ocean surrounding SESA shore. Results are almost in agreement with Figure 1 (d) from Drummond et al., 2008. The main difference arises over the central Brazil/Amazon basin, a region that in the previously mentioned study is characterized by positive values of the $(E-P)^{10}$ budget while in our case takes negative values. The difference could be associated with the reanalysis data employed to drive the FLEXPART model: while we consider the NCEP-CFSR reanalysis, Drumond et al. (2008) employed a reanalysis from ECMWF. Other factors that can introduce differences are that the

328 selected domain for SESA is not exactly the same and that we consider Dec-Jan-Feb,
329 while Drumond et al., 2008 consider Jan-Feb-Mar season.

330 Figure 5 (c) shows the difference in $(E\text{-}P)^{10}$ during the 80s and 90s that are significant at
331 10% level. It suggests that during the 80s the central-eastern shore of Brazil acted as a
332 stronger moisture source, while during the 90s the intensity of the recycling was larger.
333 Moreover, during the 90s the region at 60W between 20-25S acted as a moisture source,
334 not clearly present during the 80s. The stronger intensity of the recycling over SESA
335 during the 90s would be in agreement with the positive PCP anomalies observed on
336 Figure 2 and the anomalous vertical integral of the moisture convergence shown in
337 Figure 4(d).

338 To interpret the changes in the moisture sources we compute the Empirical Orthogonal
339 Functions (EOFs) for the net budget $(E\text{-}P)^{10}$. Figure 6 (a) shows the first EOF pattern
340 that explains the 16.5% of the $(E\text{-}P)^{10}$ variance. Its associated principal component (PC)
341 is plotted in Figure 6(b). The EOF1 pattern shows a dipole-like structure with two
342 centers of action, one located over the central-eastern and southeast Brazil, and another
343 one with opposite sign in the subtropical region located to the east of the Andes (20-
344 35)ºS, (295-305)ºE. The associated PC1 shows a clear jump between both decades of
345 study, '80s and'90s (see Figure 6(b)). Positive (negative) values of the PC1 tend to
346 prevail before 1991 (after 1991) , suggesting that the center located over the central-
347 eastern and southeast Brazil would take positive (negative) values, and therefore, the
348 particles that pass through that region along their trajectory toward SESA will load more
349 (less) moisture. This center of action is associated with the statistically significant
350 positive signal observed on Figure 5(c) over the central-eastern and southeast Brazil.
351 The other center of action of the EOF1 pattern has the opposite sign and could be
352 related to the two statistically significant negative signals observed in Figure 5(c) over

the subtropical region located to the east of the Andes. Comparing Figures 4(c) and (f) suggests that during the 80s the northerly anomalies along the coast of central-east and south Brazil associated with a cyclonic circulation at (15S, 50W) help the transport of moisture toward SESA. During the 90s the situation is the opposite: a low-level anti-cyclonic circulation developed over central-east Brazil that does not favor the advection of moisture from the central-east shore of Brazil toward SESA, decreasing the contribution of this region as a moisture source. Instead, it favours the transport of moisture from the Amazon basin and can explain the extension of the region acting as moisture source toward the north of SESA in that decade. Note that the development of this low-level cyclonic (anti-cyclonic) anomaly circulation over the central-east Brazil during the ‘80s (‘90s) is, in turn, consistent with the observed convergence anomaly of the vertical integral of moisture flux over the region shown in Figure 4(a) (Figure 4(d)).

Thus, during the 90s there is an increase in cyclonic vorticity advection in upper levels and a strong contribution of moisture from the Amazon at lower level, resulting in a larger precipitation in SESA with respect to the 80s.

6. Conclusions.

The atmosphere is sensitive to the ocean surface conditions in the tropics in such a way that SST anomalies over the tropical oceans are able to generate quasi-stationary Rossby waves that propagate from the tropics toward extratropical latitudes inducing regional circulation anomalies that can not only induce rainfall variability, but also changes in the sources of moisture. The work reported here has two complementary parts: in the first part we construct a climate network to detect synchronization periods among the tropical oceans and the precipitation over SESA during the austral summer season. Afterwards, taking into account these results, we select two periods with different

377 degree of synchronization to compare the spatial distribution of the moisture sources. To
378 do so we employ a Lagrangian particle dispersion model, that allows the calculation and
379 tracking of the trajectories of atmospheric moisture.

380 Results show that during the last century the network distance was characterized by
381 interannual and interdecadal variability having three synchronization periods among the
382 tropical oceans and the precipitation over SESA, which developed during the ‘30s, ‘70s
383 and ‘90s decades. The relationship between the mean network distance and the
384 precipitation over SESA is such that a larger degree of synchronization among the
385 network’s component (smaller mean network distance) is associated with an increase of
386 the oceanic influence on SESA precipitation.
387
388 We then focus on the differences between the ‘80s (1979-1991) and the ‘90s (1992-
389 2000), one period of non-synchronization and another of statistically significant
390 synchronization among the tropical oceans and SESA precipitation. The comparison
391 yielded the following conclusions:
392
393 1) When the synchronization of the network is statistically significant
394 (‘90s) there is convergence of moisture and favoring conditions for
395 ascent motions over SESA, allowing an increase of the SESA
396 precipitation. The opposite conditions can be observed in the period of
397 non-synchronization (‘80s) resulting in reduced rainfall.
398
399 2) The main moisture sources of SESA are the recycling over the region,
400 the central-eastern shore of Brazil together with its surrounding Atlantic

Ocean, and the southwestern south Atlantic surrounding the SESA domain.

3) The main differences between the two selected decades are in the intensity of the recycling, in the intensity of the central-eastern shore of Brazil and in a region centered at (20ºS, 300ºE). The latter is a moisture source for SESA only during the ‘90s and is associated with the development of a low-level anti-cyclonic anomaly circulation over central-east Brazil which favors the transport of moisture from that region toward SESA. On the other hand, during the ‘80s a low-level cyclonic anomaly circulation developed over central-east Brazil favors a stronger advection of moisture from the central-eastern shore of Brazil.

Acknowledgments

The research leading to these results has received funding from the European Community’s Seventh Framework Programme [FP7/2007-2011] under grant agreement nº 289447 (ITN LINC).

EHG and CL acknowledge support from FEDER and MINECO (Spain) through project ESCOLA (CTM2012-39025-C02-01).

References

Alexander, M, A.I. Blade, M. Newman, J.R. Lanzante, N.C. Lau, J.D. Scott, 2002. The atmospheric bridge: the influence of ENSO teleconnections on air–sea interaction over the global oceans. J Climate 15:2205–2231.

Andreoli, R.V., M.T. Kayano, 2005. ENSO-related rainfall anomalies in South America and associated circulation features during warm and cold Pacific decadal oscillation regimes. International Journal of Climatology, 25(15), 2017-2030.

Annamalai, H., R. Murtugudde, J. Potemra, S.P. Xie, P. Liu,B. Wang, 2003. Coupled dynamics over the Indian Ocean: spring initiation of the zonal mode. Deep Sea Research II:Tropical Studies in Oceanography, 50(12): 2305-2330.

Barreiro, M., A. Tippmann, 2008. Atlantic modulation of El Nino influence on summertime rainfall over southeastern South America. Geophysical Research Letters, 35:L16704. doi:10.1029/2008GL035019.

Barreiro, M., 2010: Influence of ENSO and South Atlantic Ocean on climate predictability over southeastern South America. Climate dynamics 35: 1493-1508. DOI: 10.1007/s00382-0666-9

Barreiro, M., N. Diaz, M. Remon, 2014. Role of the oceans and land-atmosphere interaction on summertime interdecadal variability over northern Argentina. *Climate dynamics.* 42(7-8): 1733-1753. DOI: *10.1007/s00382-014-2088-6*

Berbery, E.H., V.R. Barros, 2002. The hydrologic cycle of the La Plata basin in South America. *Journal of Hydrometeorology, 3*(6), 630-645.

Brubaker, K.L., D. Entekhabi, P.S. Eagleson,1993. Estimation of continental precipitation recycling. *Journal of Climate*, *6*(6), 1077-1089.

448 Castillo, R., R. Nieto, A. Drumond, L. Gimeno, 2014. The role of the ENSO cycle in the
449 modulation of moisture transport from major oceanic moisture sources. Water
450 Resources Research, 50(2), 1046-1058.
451

452 Chan, S.C., S.K. Behera,T. Yamagata, 2008. Indian Ocean Dipole influence on South
453 American rainfall. *Geophysical Research Letters* 35(14). L14S12. DOI:
454 10.1029/2008GL034204.

455 Dee, D.P., S.M. Uppala,A.J. Simmons, P. Berrisford,P. Poli, S. Kobayashi, U. Andrae,
456 M.A. Balmaseda,G. Balsamo,P. Bauer, P.'Bechtold, A.C.M. Beljaars, L. van de Berg,J.
457 Bidlot, N. Bormann,C. Delsol, R. Dragani,M. Fuentes, A.J. Geer, L. Haimberger, S.B.
458 Healy,H. Hersbach,E.V. Holm,L. Isaksen, P. Kallberg, M. Kohler, M. Matricardi, A.P.
459 McNally, B.M. Monge-Sanz, J.J. Morcrette, B.K.. Park, C. Peubey, P. deRosnay, C.
460 Tavolato, J.N. Thepaut, F. Vitart, 2011. The ERA-Interim reanalysis: Configuration and
461 performance of the data assimilation system. *Quarterly Journal of the Royal*
462 *Meteorological Society*, *137*(656), 553-597.
463

464 Diaz, A.F., C.D. Studzinski, C.R. Mechoso,1998. Relationships between precipitation
465 anomalies in Uruguay and southern Brazil and sea surface temperature in the Pacific
466 and Atlantic Oceans. *Journal of Climate* 11(2): 251-271.

467 Dirmeyer, P. A., K.L. Brubaker, T. DelSole, 2009. Import and export of atmospheric
468 water vapor between nations. *Journal of hydrology*, *365*(1), 11-22.
469

470 Drumond, A., J. Marengo, T. Ambrizzi, R. Nieto, L. Moreira, L. Gimeno, 2014. The
471 role of the Amazon Basin moisture in the atmospheric branch of the hydrological cycle:

a Lagrangian analysis. *Hydrology and Earth System Sciences*, *18*(7), 2577-2598. doi:10.5194/hess-18-2577-2014

.

Drumond, A., R. Nieto, L. Gimeno, T. Ambrizzi, 2008. A Lagrangian identification of major sources of moisture over Central Brazil and La Plata Basin. J. Geophys. Res., 113, D14128, doi: 10.1029/2007JD009547.

Enfield, D.B., D.A. Mayer, 1997. Tropical Atlantic sea surface temperature variability and its relation to El Niño Southern Oscillation. *Journal of Geophysical Research: Oceans.* 102: 929-945. DOI: 10.1029/96JC03296.

Grimm, A.M., V.R. Barros, M.E. Doyle, 2000. Climate variability in Southern South America associated with El Niño and La Niña events. *Journal of Climate* 13(1): 35-58.

Quadro, M.F., E.H. Berbery, M.S. Dias, D.L. Herdies, L.G. Gonçalves, 2013. The atmospheric water cycle over South America as seen in the new generation of global reanalyses. In *AIP Conference Proceedings* (Vol. 732, pp. 732-735).

Marengo, J. A. 2005. Characteristics and spatio-temporal variability of the Amazon River Basin Water Budget. *Climate Dynamics*, *24*(1), 11-22.

Martín-Gómez, V., M. Barreiro,2015. Analysis of ocean's influence on spring time rainfall variability over southeastern South America during the 20th century *Int. J. Climatology, in press*

Martinez, J. A., F. Dominguez, 2014. Sources of Atmospheric Moisture for the La Plata River Basin*. *Journal of Climate, 27*(17), 6737-6753.

Meyers, G., P. Mcintosh, L. Pigot, M. Pook,2007. The years of El Niño, La Niña and Interactions with the Tropical Indian Ocean. *Journal of Climate* 20: 2872-2880.

Nogués-Paegle, J., and K.C. Mo, 1997. Alternating wet and dry conditions over South America during summer. *Monthly Weather Review, 125*(2), 279-291.

Numaguti, A. 1999. Origin and recycling processes of precipitating water over the Eurasian continent: Experiments using an atmospheric general circulation model. *Journal of Geophysical Research: Atmospheres (1984–2012), 104*(D2), 1957-1972.

Rodriguez-Fonseca, B., I. Polo,J. Garcia-Serrano, T. Losada, E.Mohino, C.R. Mechoso, F.Kucharski, 2009. Are Atlantic Niño enhancing Pacific ENSO events in recent decades? *Geophysical Research Letters*. 36(20): L20705. DOI: 10.1029/2009GL040048.

Ropelewski, C.F., M.S,. Halpert, 1987. Global and regional scale precipitation patterns associated with the El Niño/Southern Oscillation. *Monthly weather review*, *115*(8), 1606-1626.

Saha, S., S. Moorthi, H. Pan, X. Wu, J. Wang, S. Nadiga, P. Tripp, R. Kistler, J. Woollen, D. Behringer, H. Liu, D. Stokes, R. Grumbine, G Gayno, J. Wang, Y. Hou, H. Chuang, H.H. Juang, J. Sela, M. Iredell, R. Treadon, D. Kleist, P.Van Delst, D. Keyser, J. Derber, M. Ek, J. Meng, H. Wei, R. Yang, S. Lord, H. van den Dool, A. Kumar, W.

519 Wang, C. Long, M. Chelliah, Y. Xue, B. Huang, J. Schemm, W. Ebisuzaki, R. Lin, P.
520 Xie, M. Chen, S. Zhou, W. Higgins, C. Zou, Q. Liu, Y Chen, Y. Han, L. Cucurull, R.W.
521 Reynolds, G. Rutledge, M. Goldberg, M. 2010 . NCEP Climate Forecast System
522 Reanalysis (CFSR) 6-hourly Products, January 1979 to December 2010. *Research Data,*
523 *The National Center for Atmospheric Research, Computational and Information*
524 *Systems Laboratory, Boulder, Colo, USA*. http://dx.doi.org/10.5065/D69K487J.
525 Saravanan, R., P. Chang, 2000. Interaction between Tropical Atlantic Variability and El
526 Niño – Southern Oscillation. *Journal of Climate* 13: 2177-2194.

527 Schneider, U., A. Becker, P. Finger,A. Meyer-Christoffer,B. Rudolf, Bruno, M. Ziese
528 2011. GPCC Full Data Reanalysis Version 6.0 at 1.0: Monthly Land-Surface
529 Precipitation from Rain-Gauges built on GTS-based and Historic Data. DOI:
530 10.5676/DWD_GPCC/FD_M_V6_100.
531 http://www.esrl.noaa.gov/psd/data/gridded/data.gpcc.html
532

533 Seager R, N. Naik, W. Baethgen, A. Robertson, Y. Kushnir,J. Nakamura, S. Jurburg,
534 2010. Tropical Oceanic Causes of Interannual to Multidecadal Precipitation Variability
535 in Southeast South America over the past Century. *Journal of Climate*. 23: 5517-5539.
536 Doi: 10.1175/2010JCLI3578.1.

537 Silva, G.A., T. Ambrizzi, J.A. Marengo, 2009. Observational evidences on the
538 modulation of the South American Low Level Jet east of the Andes according the
539 ENSO variability. In *Annales geophysicae* 27(2), 645 – 657. Copernicus GmbH.
540

541 Silvestri, G.E. 2004. El Niño signal variability in the precipitation over southeastern
542 South America during the austral summer. *Geophysical Research Letters* 31(18). DOI:
543 10.1029/2004GL020590.

544 Smith, T.M., R.W. Reynolds, and T.C. Peterson, J. Lawrimore, 2008. Improvements to
545 NOAA's Historical Merged Land-Ocean Surface Temperature Analysis (1880-2006).
546 *Journal of Climate.*, 21, 2283-2296.
547
548 Stohl, A., C. Forster, A. Frank, P. Seibert, G. Wotawa, 2005. Technical note: The
549 Lagrangian particle dispersion model FLEXPART version 6.2. *Atmospheric Chemistry*
550 *and Physics*, *5*(9), 2461-2474.
551
552 Stohl, A., P. James 2004, A Lagrangian analysis of the atmospheric branch of the global
553 water cycle. part I: Method description, validation, and demonstration for the August
554 2002 flooding in central Europe, J. Hydrometeorol., 5, 656–678.
555
556 Stohl, A., P. James 2005, A Lagrangian analysis of the atmospheric branch of the global
557 water cycle. part II: Earth's river catchments, ocean basins, and moisture transports
558 between them, J. Hydrometeorol., 6, 961–984.
559
560 Tsonis, A.A., K. Swanson, S. Kravtsov, 2007. A new dynamical mechanism for
561 majorclimate shifts. *Geophysical Research Letters* 34(13): L13705.
562 DOI: 10.1029/2007GL030288.
563
564 Vera, C., G. Silvestri, V. Barros, A. Carril, 2004. Differences in el nino response over
565 the southern hemisphere. *Journal of Climate*, *17*(9), 1741-1753.
566
567 Vera, C., W. Higgins, J. Amador, T. Ambrizzi, R. Garreaud, D. Gochis, D. Gutzler, D.
568 Lettenmaier, J. Marengo, S.R. Mechoso, J. Nogues-Peagle, P.L. Silva Diasand C. Zhang

2006. Toward a unified view of the American monsoon systems. *Journal of Climate*, *19*(20), 4977-5000.

Viviane B.S. Silva Vernon E. Kousky (2012). The South American Monsoon System: Climatology and Variability, Modern Climatology, Dr Shih-Yu Wang (Ed.), ISBN: 978-953-51-0095-9, InTech, DOI: 10.5772/38565. Available from: http://www.intechopen.com/books/modern-climatology/the-south-american-monsoon-system-climatology-and-variability

Wang, X., C. Wang, 2014. Different impacts of various El Niño events on the Indian Ocean Dipole. *Climate dynamics* 42: 991-1005

Wu, R., B.P, Kirtman, 2004. Understanding the Impacts of the Indian Ocean on ENSO Variability in a Coupled GCM. *Journal of Climate* 17: 4019-4031.

Xue, Y., T.M. Smith, R.W. Reynolds, 2003. Interdecadal changes of 30-yr SST normal during 1871-2000 *Journal of Climate,* 16, 1601-1612.

Yoo, G.H., J.S. Kug, J.Y. Park, F.F. Jin, 2013. Sea surface temperature in the north tropical Atlantic as a trigger for El Niño/Southern Oscillation events. *Nature Geoscience* 6:112-116. Doi: 10.1038/NGEO1986.

Yoon, J.H., N. Zeng, 2010. An Atlantic influence on Amazon rainfall. Climate dynamics, 34(2-3), 249-264.

Zemp, D.C., C.F. Schleussner, H.M.J. Barbosa, R.J. Van der Ent, J.F. Donges, J. Heinke, G. Sampaio, A. Rammig,2014. On the importance of cascading moisture recycling in South America. *Atmospheric Chemistry and Physics*, *14*(23), 13337-13359.

593

594

595 **List of Tables:**

596 **Table 1:** Geographical regions of each index that make up our network's nodes. The
597 indices are defined considering the spectral average of the sea surface temperature (for
598 TNA, NINO3.4, TSA, ATL3 and IOD) and precipitation (for PCP) anomalies in the
599 specified regions. In the Indian Ocean Dipole case, the index is computed from the
600 difference between the 2-D average SST in the west region and the 2-D average in the
601 east region. Land areas are only considered for the case of the precipitation index.

602 **List of Figures:**

603 **Figure 1**. Regions that represent the spatial domain over which the SST anomalies (over
604 the oceans) and PCP anomalies (over the continent) are averaged to define the climate
605 indices (or network's nodes).

606 **Figure 2**. Mean network distance time series during the 20th century computed from Eq.
607 (1) (solid black curve). To compute this time series, Niño3.4 is centered on Septiember-
608 October-November; TNA, TSA, ATL3, IOD and PCP are centered on DJF (December-
609 January-March). The shaded black line represents the precipitation index over SESA in
610 austral summer and the horizontal black dot line represents the 5% significance level
611 below which the distance identifies significant synchronization. Each point of the
612 network distance time series represents the value of the mean network distance
613 computed considering a sliding window of 11 years length $[t-\frac{\Delta t}{2}, t+\frac{\Delta t}{2}]$ centered on
614 year t.

615 **Figure 3**. Spearman correlation maps between the PCP index over SESA and the SST
616 anomalies centered on the austral summer season (December-January-February) for (a)
617 '80s decade and (b) '90s decade. The anomaly values were computed considering the
618 deviation from the climatological period (1901-2005). The colored domains represent
619 those regions which are statistically significant at 95% significance level in a
620 MonteCarlo test based on the generation of 100 surrogate time series.

621 **Figure 4**. Anomaly vertical integral divergence moisture flux (VIDMF) in $kg \cdot m^{-2}s^{-2}$ for:
622 (a) (1979-1991) and (d) (1992-2000). Anomaly eddy geopotential (geopot) at 200mb in
623 m^2s^{-2} for: (b) (1979-1991) and (e) (1992-2000). Anomaly winds at 850mb in m/s for (c)
624 (1979-1991) and (f) (1992-2000). To compute (b) and (e) maps, we first remove the
625 trend from 1979 to 2005 and the zonal average of the geopotential at 200mb. After that
626 we remove the climatology of the period (1979- 2005) and apply the low-pass the
627 Lanczos filter to the time series. From this anomalies values we finally select DJF
628 season and make an average over the periods: (1979-1991) and (1992-2000). To
629 compute the (a), (d), (c) and (f) maps we remove the trend and the climatology mean
630 from 1979 to 2005 and apply the Lanczos filter to the time series Then we compute the
631 DJF average for each period to obtain the anomalies. The marked region over South
632 America represents the domain where the PCP over SESA index was defined.

633 **Figure 5**. (a) 10 days average of the net budget evaporation minus precipitation ((E-
634 $P)^{10}$) during the 80s (1979-1991) in DJF, (b) the same in the 90s (1992-2000) . (c)
635 Difference between the 80s and 90s. Only locations with difference significant at 90%
636 confidence level considering a Monte Carlo approach are colored. Units: mm/day

637 **Figure 6**. (a) First EOF of $(E-P)^{10}$ and (b) its associated PC1. Period (1979-2000).

638

Index short name	Index long name	Earth's regions	
		Latitude range	**Longitude range**
NINO3.4	El Niño3.4	5ºN-5ºS	170ºW-120ºW
TNA	Tropical North Atlantic	10ºN-30ºN	60ºW-30ºW
TSA	Tropical South Atlantic	5ºS-25ºS	330ºE-358ºE
ATL3	Equatorial Atlantic	3ºN-3ºS	0ºW-20ºW
IOD	Indian Ocean Dipole	10ºS-10ºN 10ºS-0ºN	50ºE-70ºE 90ºE-110ºE
PCP	Precipitation Southeastern South America (SESA). (only land areas are considered)	25ºS-40ºS	60ºW-50ºW

Figure 1

Click here to download Rendered Figure Figure1.tif

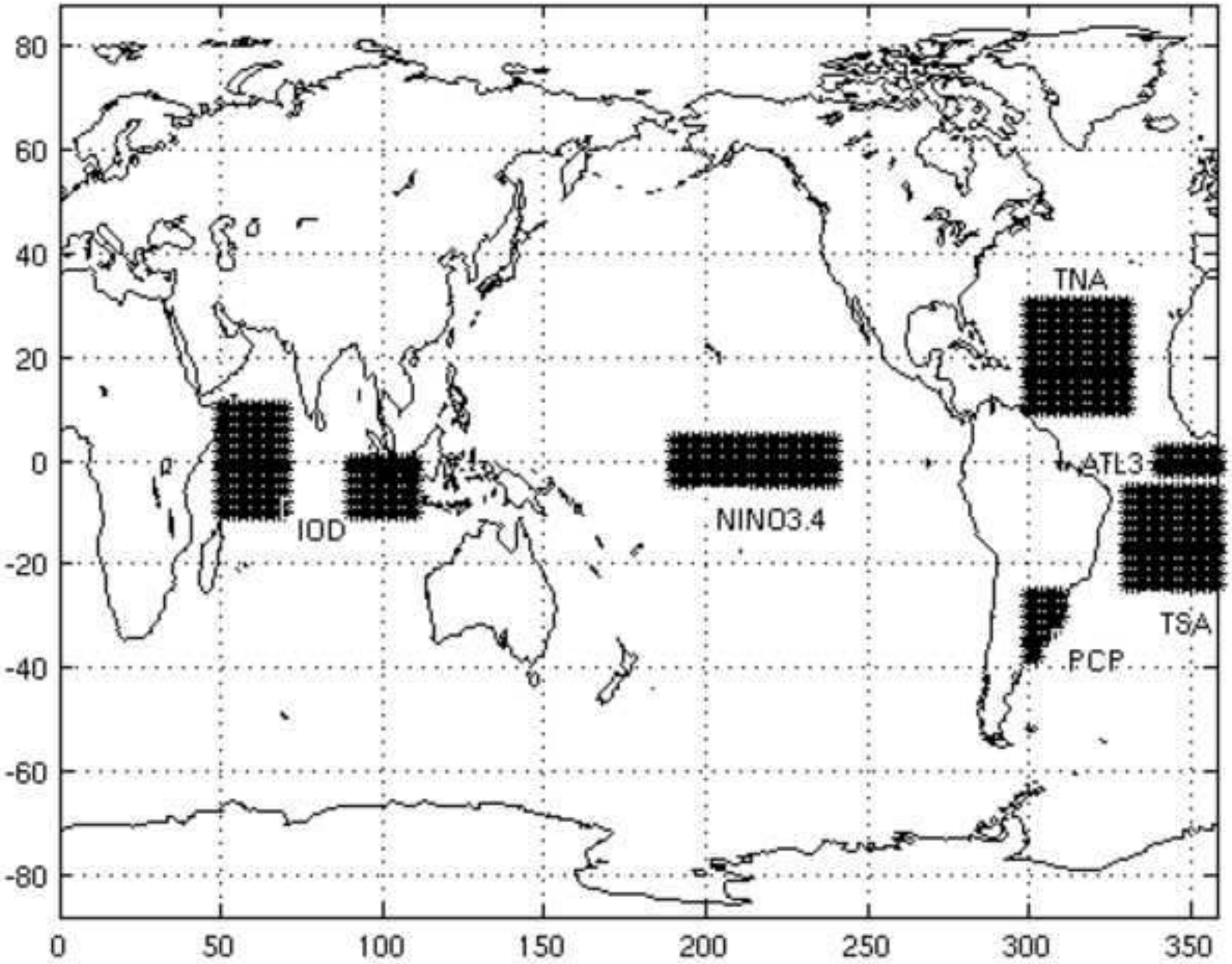

Figure 2

Click here to download Rendered Figure Figure2_paper3.tiff

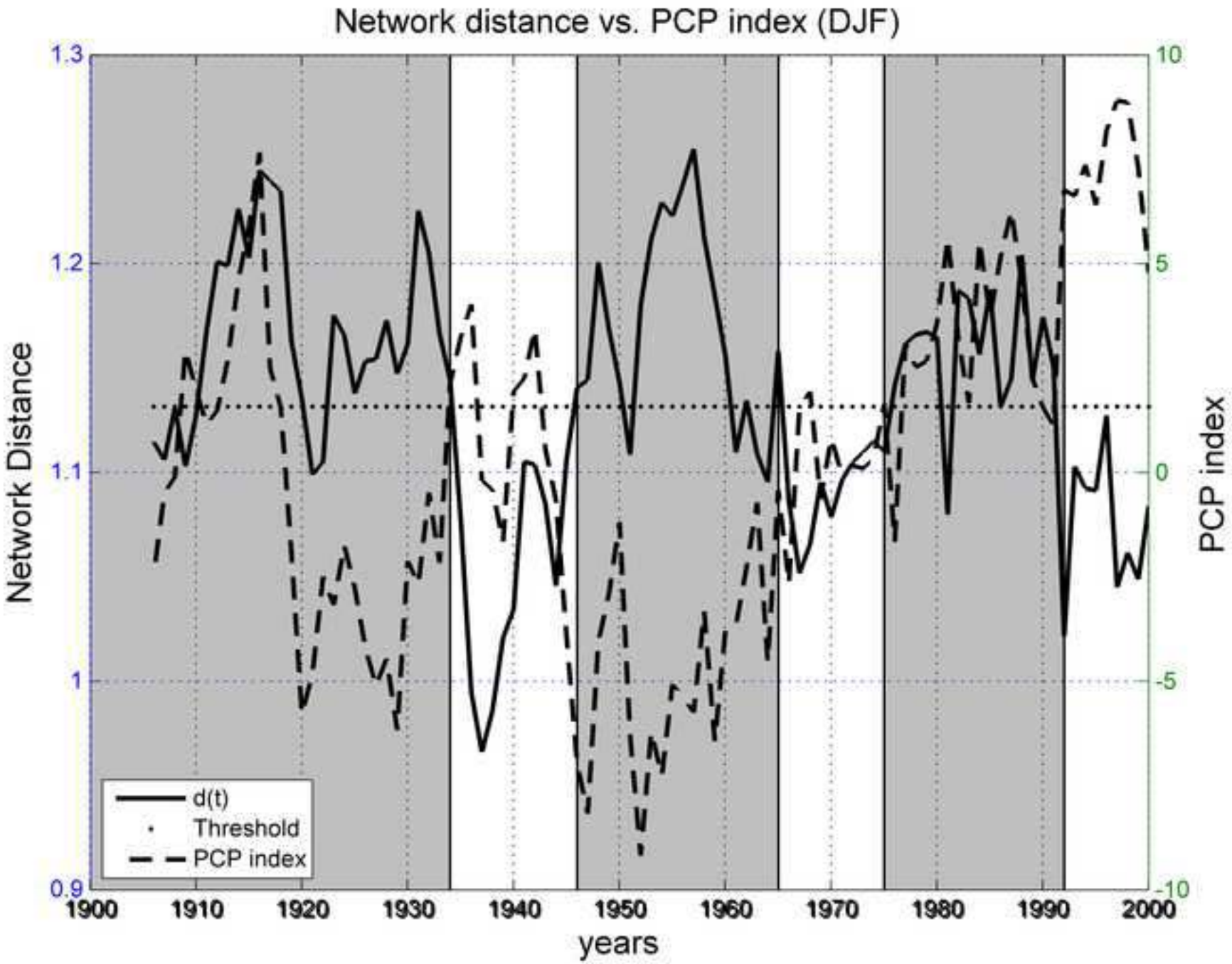

Figure 3

Click here to download Rendered Figure Figure3_paper3.tiff

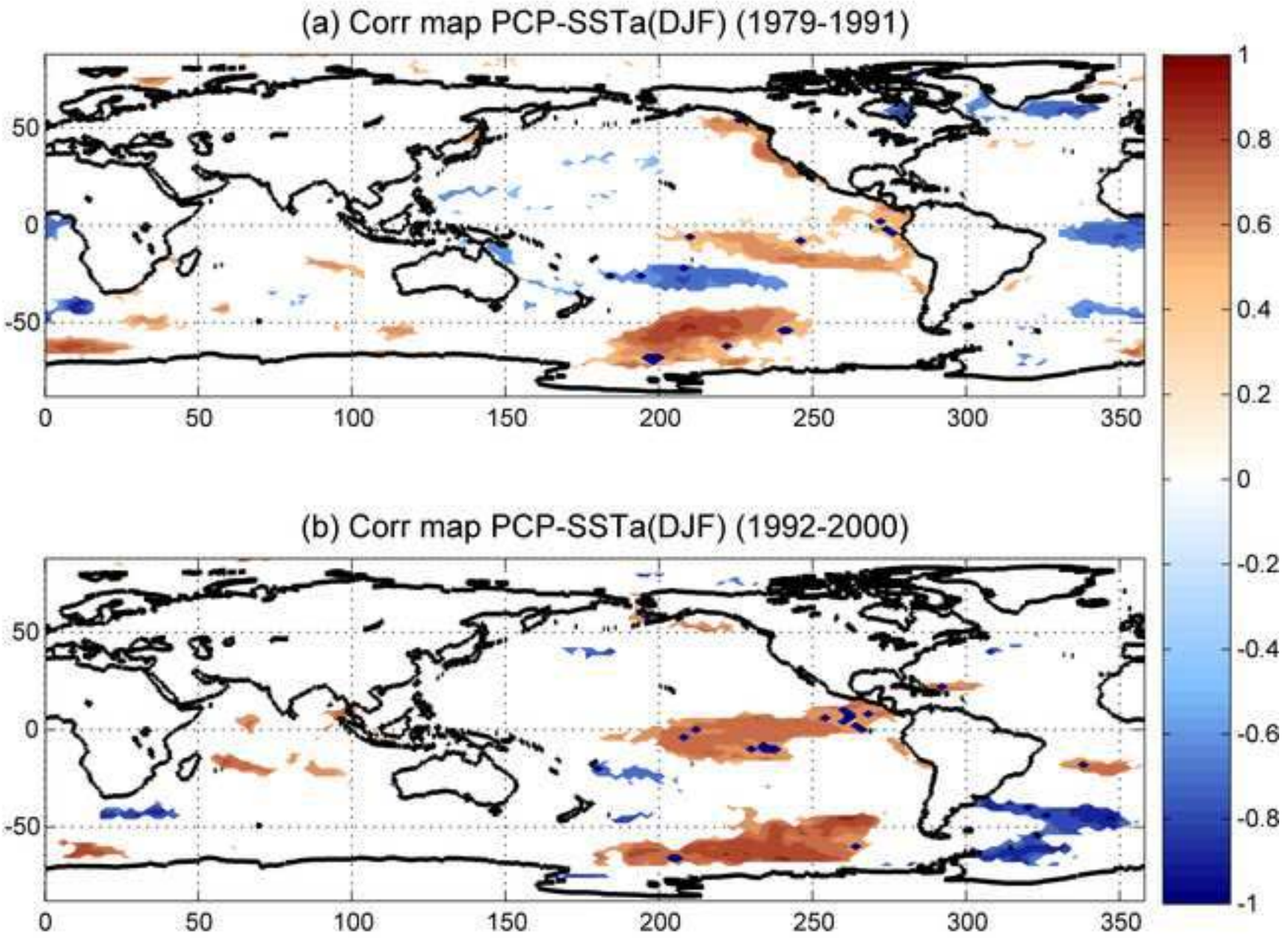

Figure 4

Click here to download Rendered Figure Figure4BIS_paper3.tiff

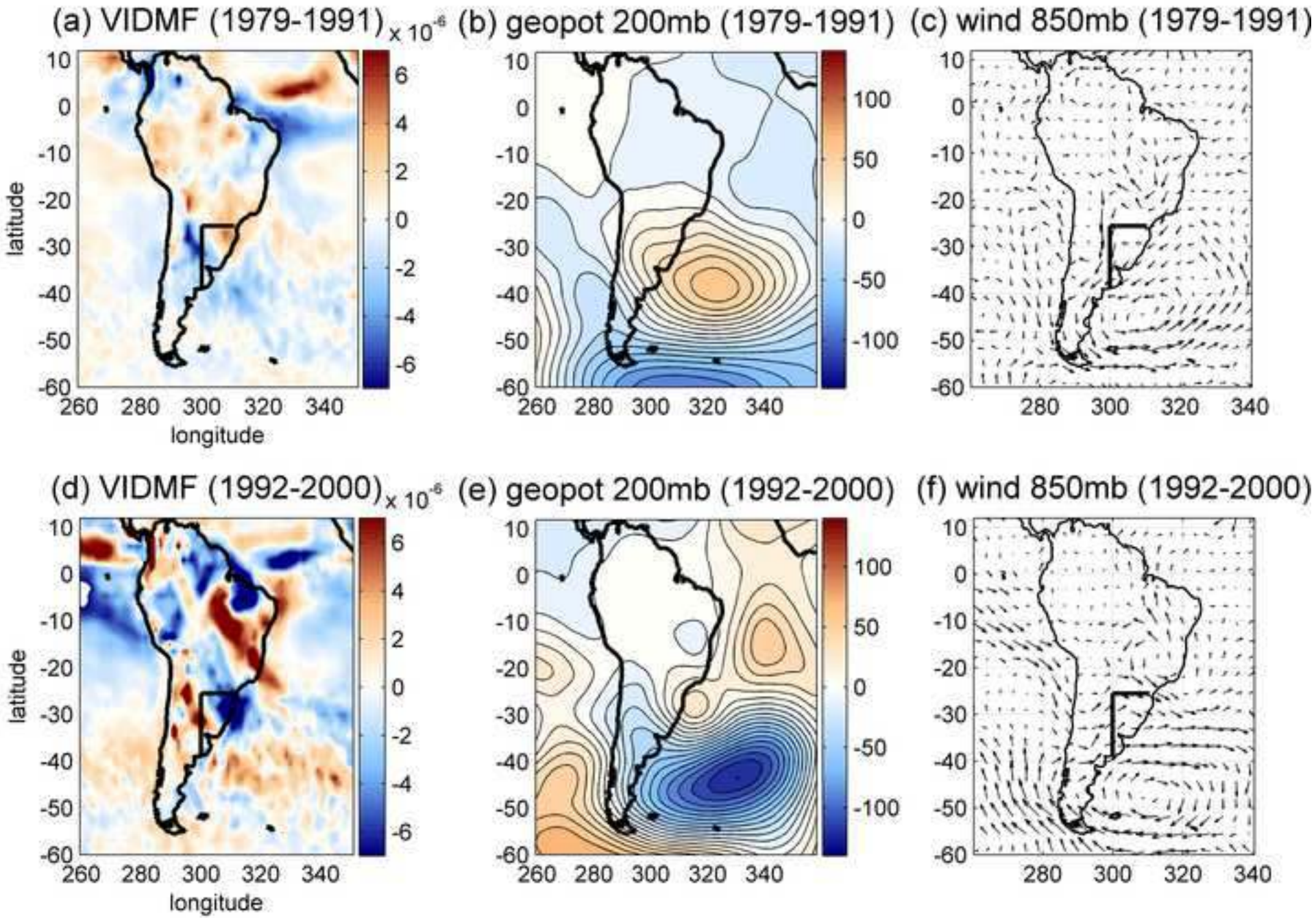

Figure 5

Click here to download Rendered Figure Figure5_paper3.tiff

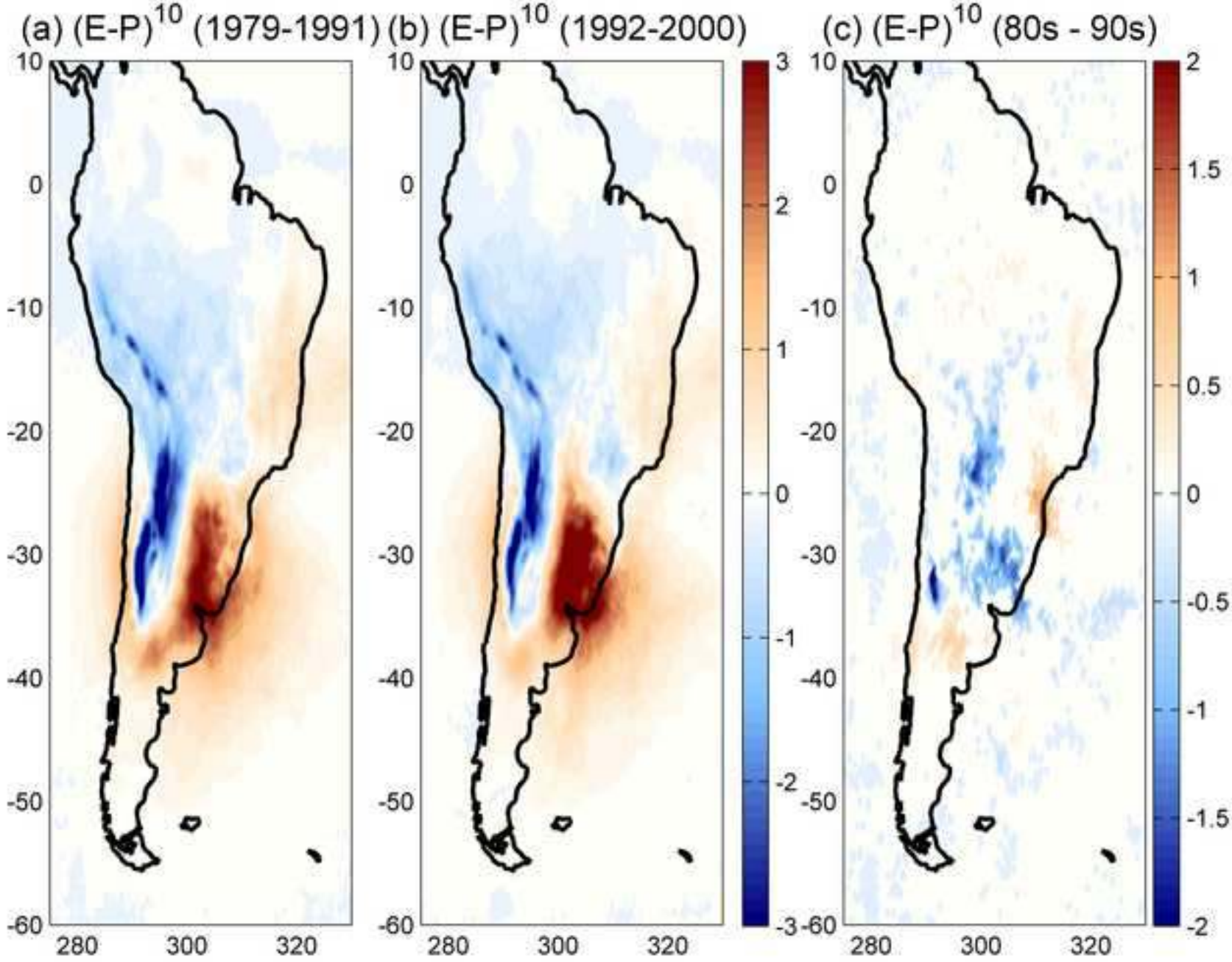

Figure 6